



Contents lists available at ScienceDirect



# Catalysis Today

journal homepage: [www.elsevier.com/locate/cattod](http://www.elsevier.com/locate/cattod)

## Mesoporous silico-aluminophosphates derived from microporous precursors as promising catalyst for hydroisomerization

Rekha Yadav, Arvind Kumar Singh, Ayyamperumal Sakthivel\*

Inorganic Materials and Catalysis Laboratory, Department of Chemistry, University of Delhi, Delhi 110 007, India

### ARTICLE INFO

#### Article history:

Received 30 November 2013

Received in revised form 14 August 2014

Accepted 16 September 2014

Available online xxx

#### Keywords:

Hydroisomerization

1-Octene

SAPO-37

SAPO-34

SAPO-5

Mesoporous silicoaluminophosphates

Faujasite

Secondary building units

### ABSTRACT

A series of mesoporous silicoaluminophosphates (MESO-SAPOs) with different silica contents were synthesized using the microporous precursors of SAPO-37 (MESO-SAPO-37). Various analytical and spectroscopic techniques revealed the presence of mesoporous and microporous properties of the materials. The resulting materials were applied to vapor-phase hydroisomerization of 1-octene to afford the corresponding branched alkenes in good yields under ambient conditions. The catalytic activity of MESO-SAPO-37 was compared to those of other mesoporous analogs obtained from SAPO-34 and SAPO-5 precursors. Among all the synthesized materials, MESO-SAPO-37 showed the best catalytic activity owing to the presence of faujasite units.

© 2014 Elsevier B.V. All rights reserved.

### 1. Introduction

Isomerization of linear alkanes/alkenes to the corresponding iso-alkanes/alkenes is an important transformation in terms of increasing the octane count of fuel. The process was developed during World War II to increase the octane number of gasoline [1] and is important in the petrochemical industry and fine chemical synthesis [2]. Earlier, isomerization reactions were carried out using homogeneous Friedel–Crafts-type acid catalysts [3]; however, these catalysts suffer from drawbacks such as handling difficulty, generation of a large amount of waste and its disposal, and regenerability of catalysts. These limitations can be overcome by replacing homogeneous catalysts with heterogeneous solid-acid catalysts, including zeolite, microporous aluminophosphate (AlPO), and other solid-acid catalysts [4–6]. Besides a heterogeneous phase, microporous solid-acid catalysts have several advantages such as ion exchange and high sorption properties; they also possess enhanced structural diversity in which Al can be substituted with different metal species to fine-tune interfacial acidity and catalytic properties [7–9]. The silica-substituted AlPOs, namely, SAPO-*n* (where “*n*” represents a distinct structure

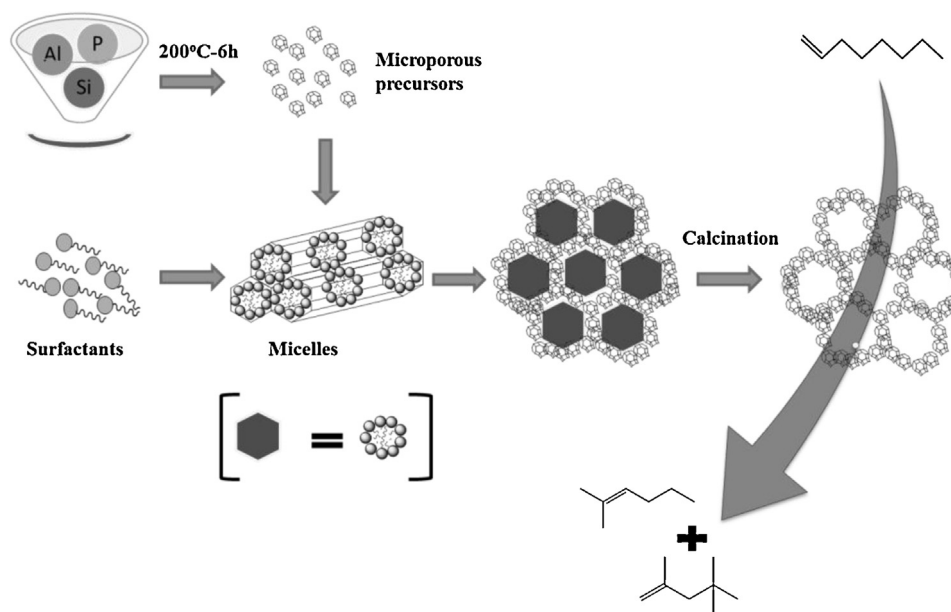
type), are relatively less acidic than zeolites [10] and provide mainly moderately acidic sites appropriate for isomerization reactions. The introduction of diverse metals to different SAPO-*n* systems afforded good isomeric yields [11–15]. However, these catalysts suffer from pore blockage and pore-size limitation for bulkier reactant molecules. The discovery of mesoporous materials containing pores with diameters between 2 and 50 nm [16–21] provided a new array of materials with large pore-size distribution. These materials showed good results in the fields of separation, adsorption, support, and heterogeneous catalysis [22–26].

In 1998, Montoya-Urbina et al. synthesized SAPO-5 system in presence of a surfactant, cetyltrimethylammonium bromide (CTAB), and reported better conversion for the isomerization of *m*-xylene compared to the systems synthesized without surfactant [27]. In continuation to the study, many researchers have tried to fine-tune the intrinsic properties of SAPO-*n* system by introducing surfactants during the synthesis and achieved good isomeric yields [28–31]. The surfactant-directed resulting materials are mesoporous with interparticle mesopores. In this regard, we recently synthesized a series of mesoporous SAPOs from microporous precursors to enhance the access to active sites [32–34]. Notably, faujasite-type aluminosilicates and SAPOs have great potential for use as fluid catalytic cracking (FCC) catalysts in gasoline upgrading and other isomerization reactions [13,35].

This study focuses on the faujasite-type SAPO-37 precursors assembled over surfactant assemblies for the synthesis of

\* Corresponding author. Tel.: +91 8527103259.

E-mail addresses: [sakthiveldu@gmail.com](mailto:sakthiveldu@gmail.com), [asakthivel@chemistry.du.ac.in](mailto:asakthivel@chemistry.du.ac.in)  
(A. Sakthivel).



**Scheme 1.** Schematic representation for formation of MESO-SAPO-*n* from corresponding microporous precursors and its application on hydroisomerization of 1-octene.

mesoporous SAPOs (MESO-SAPO-37) as shown in [Scheme 1](#). The detailed catalytic activity of these materials was compared for the vapor-phase hydroisomerization of 1-octene.

## 2. Experimental

### 2.1. Synthesis of materials

Pseudoboehmite (76%  $\text{Al}_2\text{O}_3$ ; ACE, India), fumed silica (Aerosil-200; Sigma-Aldrich), orthophosphoric acid (85%, Merck), cetyltrimethylammonium bromide (99%; Spectrochem), 25 wt.% tetramethylammonium hydroxide in water (25 wt.%; Tritech chemical) and 40 wt.% tetrapropylammonium hydroxide in water (40 wt.%; Tritech chemical) were used in the synthesis.

A series of MESO-SAPO-37 with different silica contents was prepared as per the procedure described elsewhere [32]. The molar composition used for MESO-SAPO-37 synthesis was: 1.0( $\text{TPA}$ )<sub>2</sub>O; 2.1–2.8( $\text{TMA}$ )<sub>2</sub>O; 1.0  $\text{Al}_2\text{O}_3$ ; 1.0  $\text{P}_2\text{O}_5$ ;  $x\text{SiO}_2$ ; 0.40–0.60 CTAB; and 226.94  $\text{H}_2\text{O}$ , where  $x=0.43, 0.50, 0.60$  and  $0.80$ . The synthesis of mesoporous silicoaluminophosphate involved two steps, where first step comprises the synthesis of microporous precursors and the second step involves assembly of the preformed microporous precursors into mesoporous silicoaluminophosphate in presence of a surfactant solution.

#### 2.1.1. Synthesis of microporous SAPO-37 precursor

The first step involved the formation of microporous SAPO-37 precursor as per the following procedure, with the molar gel composition 1.0  $\text{Al}_2\text{O}_3$ :1.0  $\text{P}_2\text{O}_5$ :0.43  $\text{SiO}_2$ :1.0 ( $\text{TPA}$ )<sub>2</sub>O:0.025 ( $\text{TMA}$ )<sub>2</sub>O:50.0  $\text{H}_2\text{O}$ . Solution A was prepared by slowly adding 5.25 g Pseudoboehmite alumina to a solution of 9.223 g of 85 wt.% phosphoric acid and 10 g of  $\text{H}_2\text{O}$ . The resultant solution was stirred for 8 h. Solution B was prepared by adding a calculated amount of fumed silica into the mixture containing an appropriate amount of tetramethylammonium hydroxide ( $\text{TMAOH}$ ; 25 wt.%) and tetrapropylammonium hydroxide ( $\text{TPAOH}$ ; 40 wt.%). Solution B was added drop-wise to solution A, and the final mixture was stirred for 24 h. The resultant homogeneous mixture was allowed to crystallize at 200 °C for 6 h to get SAPO-37 precursor containing microporous secondary building units. For comparison, completely

crystallized microporous SAPO-37 was obtained by 22 h crystallization.

#### 2.1.2. Conversion of SAPO-37 precursor into MESO-SAPO-37

To assemble MESO-SAPO-37 from microporous SAPO-37 precursors, the latter was introduced into the surfactant solution at an appropriate concentration. An additional quantity of tetramethylammonium hydroxide (25 wt.%) was added to the above mixture and the resultant solution was allowed to age at 90 °C for 36 h to obtain MESO-SAPO-37. Mesoporous silicoaluminophosphate prepared with different amounts of silica (0.43, 0.50, 0.60 and 0.80 M) are represented as MESO-SAPO-37-0.43S, MESO-SAPO-37-0.50S, MESO-SAPO-37-0.60S and MESO-SAPO-37-0.80S, respectively. All the as-synthesized samples were calcined in air at 550 °C for 6 h to remove organic molecules. Similarly, MESO-SAPO-34 and MESO-SAPO-5, i.e. mesoporous silicoaluminophosphates assembled using corresponding microporous precursors of SAPO-*n*, were prepared as per the composition specified in [Table 1](#).

## 2.2. Characterization

Powder X-Ray diffraction patterns of all the materials were collected on BrükerD8 diffractometer with  $\text{Cu}-\text{K}\alpha$  radiation ( $\lambda=1.54184\text{\AA}$ ), between  $2\theta$  range of 1.5° and 40°, with a scan speed and step size of 0.5°/min and 0.02° respectively. FTIR spectra were measured on PerkinElmer FTIR 2000 in 400–4000  $\text{cm}^{-1}$  range using KBr pellets. The textural properties of materials like surface area (BET, DFT), micropore area (*t*-plot method), pore volume (BJH) and pore size distribution (BJH, DFT and HK) were derived from  $\text{N}_2$  adsorption-desorption measurements carried out at –196 °C using an automatic micropore physisorption analyzer (Micromeritics ASAP 2020, USA) after the samples were degassed at 300 °C for at least 10 h under  $10^{-3}$  Torr pressure prior to each run. The morphology and size of the materials were further analyzed using a Phillips Technai G230 TEM operated at 300 kV.

The pyridine FT-IR spectra were collected with a Thermo Scientific Nicolet 6700 FTIR single beam spectrometer using a liquid nitrogen-cooled MCT detector. Pyridine vapor adsorption was carried out in a Harrick Scientific HVC-DR2 reaction chamber with a detachable ZnSe window dome mounted inside a Harrick DRA-2

**Table 1**

Textural properties of different mesoporous and microporous silicoaluminophosphate materials.

Sample name	Al:P:Si	Surface area ( $\text{m}^2/\text{g}$ )		BJH pore volume ( $\text{cm}^3/\text{g}$ )	Average desorption pore diameter (nm)		
		BET	DFT		BJH	H-K	DFT
MESO-SAPO-37-0.43S	1:1.00:0.215	458	555	0.33	3.1	1.5	0.88
MESO-SAPO-37-0.80S	1:1.00:0.400	426	445	0.31	3.7	1.6	1.2
MESO-SAPO-34	1:1.06:0.540	448	587	0.47	2.9	1.5	0.88
MESO-SAPO-5	1:1.00:0.100	487	655	0.39	3.1	1.6	0.88
SAPO-37	1:1.00:0.215	146	—	0.15	—	—	—
SAPO-34	1:1.06:0.540	246	—	0.22	—	—	—
SAPO-5	1:1.00:0.100	155	—	0.13	—	—	—

Praying Mantis diffuse-reflectance accessory designed to minimize parasite specular reflectance. About 100 mg (10% of sample was mixed with KBr) of sample was placed in the sample cup and was pre-activated at 350 °C for 6 h. For pyridine adsorption, helium gas was passed through a pyridine saturator. A partial pressure of 27 mmHg of pyridine was maintained in the saturator. After pyridine adsorption, the sample was heated to 150 °C with ultra-high pure helium flush for 1 h to ensure that the physically adsorbed pyridine was recovered completely. Sample spectrum was collected with KBr background once the sample temperature reached 25 °C. Subsequently, the sample was degassed at a desired temperature and spectra were collected at different temperatures. Thermal gravimetric analysis (TGA) and differential thermo gravimetric analysis (DTA) of spent catalyst was carried out on PerkinElmer. About 5–10 mg of sample was heated in air with rate 10 °C/min from 21 °C to 1200 °C. Diffuse reflectance infrared (DRIFT-IR) spectra of spent catalyst have been recorded on Brüker optic model tensor 27 FT-IR spectrometer. It is equipped with gold coated cube corner mirror optics and Harrick Mantis diffused reflectance accessory. The spectra were recorded in absorbance mode with 64 scans per sample.

### 2.3. Catalytic studies on hydroisomerization of 1-octene

1-Octene (Sigma-Aldrich, 98%) hydroisomerization was studied using a fixed-bed reactor (Chemitco, India) under hydrogen flow. The flow of hydrogen was controlled using an Aalborg mass flow controller. Prior to each catalytic activity measurement, the catalysts were activated in air at 400 °C for 6 h. A wide range of reaction conditions was studied, including temperature from 300 to 450 °C and different WHSV = 5, 8, and 12 h<sup>-1</sup>. The products were analyzed using gas chromatography connected to a HP-5 capillary column (Agilent 7890A series).

## 3. Results and discussion

### 3.1. Materials characterization

Fig. 1 shows the Fourier transform infrared (FT-IR) spectra of the mesoporous SAPO materials obtained from various microporous precursors and the corresponding microporous analogs. Both the microporous and mesoporous analogs showed asymmetric stretching  $\sim 1080 \text{ cm}^{-1}$  corresponding to the framework vibrational bands of Al-O-P and Si-O-Al units. The microporous materials exhibited well resolved vibrational bands at 535, 565, 756  $\text{cm}^{-1}$  for SAPO-37, 530, 560,  $\text{cm}^{-1}$  for SAPO-34 and 560, 630  $\text{cm}^{-1}$  for SAPO-5 respectively are typical of crystalline structural framework unit. MESO-SAPO-37, MESO-SAPO-5, and MESO-SAPO-34 showed vibrational bands in the region 530–565  $\text{cm}^{-1}$  [32,36,37], 530–630  $\text{cm}^{-1}$  [38], and 526–640  $\text{cm}^{-1}$  [34,39,40], respectively, representing the structural secondary building units of SAPO-37, SAPO-5, and SAPO-34, respectively (Fig. 1). The vibrational bands in the mesoporous

analogs are relatively broad compared to those of the microporous analogs, indicating that the secondary building units are discrete and present on the walls of mesoporous channels. It is evident from the spectra that all the materials were assembled from the preformed microporous materials possessing structural subunits of the corresponding SAPO-*n* on the walls of mesoporous channels.

The powder X-ray diffraction (XRD) patterns for MESO-SAPO-37 with different silica contents are shown in Fig. 2. All the samples show well-resolved reflection at a 2θ angle of  $\sim 2^\circ$ , corresponding to the (100) plane of the hexagonal mesoporous phase. The observed 2θ values of MESO-SAPO-37 for the (100) plane are 2.25°, 2.24°, 2.19°, and 2.09° for MESO-SAPO-37-0.43S, MESO-SAPO-37-0.50S, MESO-SAPO-37-0.60S, and MESO-SAPO-37-0.80S, respectively. The corresponding unit cell value “a” obtained based on (100) plane possesses a value of 3.9 nm, 3.9 nm, 4.0 nm and 4.2 nm, the increase in unit cell value (shift in the 2θ values towards lower angle) with increase in silica content can be attributed to the incorporation of more amount of large tetravalent silicate ions ( $\text{Si}_4^{4+}$ , 0.04 nm) in the framework position of smaller pentavalent phosphorous sites ( $\text{P}^{5+}$ , 0.03 nm) [41]. Moreover, the low-angle powder XRD of mesoporous SAPOs assembled from other microporous precursors (MESO-SAPO-5 and MESO-SAPO-34) showed relatively broad reflection with 2θ values of 1.7° and 2.1° for MESO-SAPO-5 and MESO-SAPO-34, respectively, typical of hierarchical MCM-41-type (MCM = mobile crystalline material) hexagonal mesoporous structure. The powder XRD patterns of the representative calcined samples obtained from MESO-SAPO-37, MESO-SAPO-5, and MESO-SAPO-34 (Fig. 3) exhibited broad peaks at 2.5°, 1.8°, and 2.5°, respectively, indicating that the hierarchical mesoporosity remained intact. Moreover, the d-spacing of the

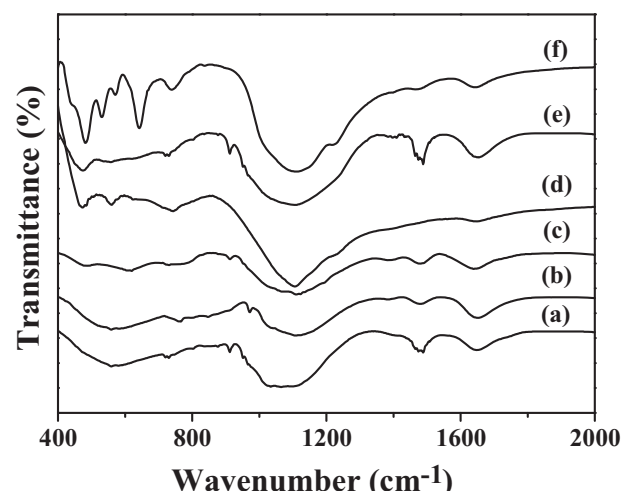
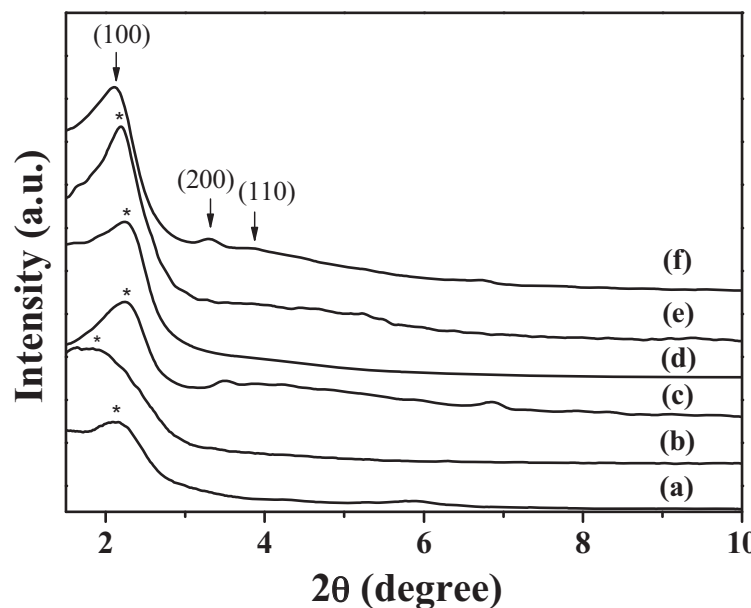


Fig. 1. FTIR of (a) MESO-SAPO-37 (b) SAPO-37, (c) MESO-SAPO-5, (d) SAPO-5, (e) MESO-SAPO-34 and (f) SAPO-34.



**Fig. 2.** XRD pattern of as-synthesized (a) MESO-SAPO-34, (b) MESO-SAPO-5, (c) MESO-SAPO-37-0.43S, (d) MESO-SAPO-37-0.50S, (e) MESO-SAPO-37-0.60S, and (f) M-S-37-0.80S.

(100) plane decreased after the calcination, indicating structural shrinkage due to the presence of highly cross-linked microporous SAPO wall [42]. Further broadening in the XRD reflection after the calcination indicates that the mesopores are of hierarchical nature. The XRD patterns in the higher  $2\theta$  region from  $10^\circ$  to  $40^\circ$  for MESO-SAPO-37-0.43 (the inset of Fig. 3) showed weak reflections  $\sim 18^\circ$ ,  $20^\circ$ ,  $21^\circ$ , and  $23^\circ$ , confirming the presence of microporous SAPO-37 units within the system (the inset of Fig. 3).

The  $N_2$ -sorption isotherms of the materials with different silica contents are shown in Fig. 4A. All the samples show both microporous and mesoporous features with type IV isotherm and H3-type hysteresis loop [43–46]. The sharp uptake at a relative pressure ( $p/p_0$ )  $< 0.1$  indicates the presence of microporous secondary building units on the walls of mesoporous structures. In the relative pressure range 0.4–0.6, multilayer adsorption with capillary condensation indicates the presence of mesoporosity in the materials. H3 hysteresis loops correspond to narrow slit-type pores,

which are typical of ordered hierarchical mesopores [43]. Fig. 4B shows the pore-size distributions of MESO-SAPO-37 synthesized with different silica contents. As the silica content increased from 0.43 to 0.5, 0.6, and 0.8, bi-model distribution appeared. MESO-SAPO-5 and MESO-SAPO-34, obtained from microporous SAPO-5 and SAPO-34 precursors, showed similar adsorption isotherms (not shown here) and uniform pore-size distributions [33,34]. The textural properties of mesoporous SAPO derived from microporous precursors are summarized in Table 1. Clearly, the samples possessed a high surface area in the range  $350$ – $450 \text{ m}^2 \text{ g}^{-1}$  with a pore volume of  $0.3$ – $0.4 \text{ cm}^3$ , indicating the typical mesopore range [31–34]. The high density functional theory (DFT) surface area observed is representative of the composite nature of materials [33]. The surface properties and composition of microporous SAPO-*n* prepared for the comparison are summarized in Table 1 and showed surface area in the range of  $110$ – $250 \text{ m}^2 \text{ g}^{-1}$  with a pore volume of  $0.13$ – $0.22 \text{ cm}^3$  which is characteristic of microporous materials. The high-resolution transmission electron microscopy (HRTEM) images of the calcined MESO-SAPO-*n* prepared from different precursors are shown in Fig. 5. All the samples show hierarchical mesoporosity with hexagonal morphology, consistent with the XRD studies. The TEM images clearly show the absence of bulk microporous phase, indicating successful assembly of mesopores from microporous precursors.

The surface acidities of MESO-SAPO-37-0.43S, MESO-SAPO-5, and MESO-SAPO-34 were studied using pyridine desorption FTIR. All the samples show (Fig. 6) broad vibrational bands  $\sim 1450$  and  $1540 \text{ cm}^{-1}$  for pyridine bound to protons/Lewis acidic sites and Brønsted acidic sites, respectively [24,25]. In all the cases, as the desorption temperature increased from  $100^\circ\text{C}$  to  $500^\circ\text{C}$ , the intensity of pyridine bound to Brønsted acidic sites remained comparable (Fig. 6) [25,26,32,47], indicating the presence of strong Brønsted acidic sites. In particular, MESO-SAPO-37 possessed strong Lewis acidic sites along with Brønsted acidic sites. In contrast, for MESO-SAPO-34, as the desorption temperature increased from  $200^\circ\text{C}$  to  $500^\circ\text{C}$ , the intensity of pyridine bound to Lewis acidic sites decreased, indicating the presence of weak Lewis acidic sites [33], whereas MESO-SAPO-5, mainly contains strong Brønsted acidic sites [34].

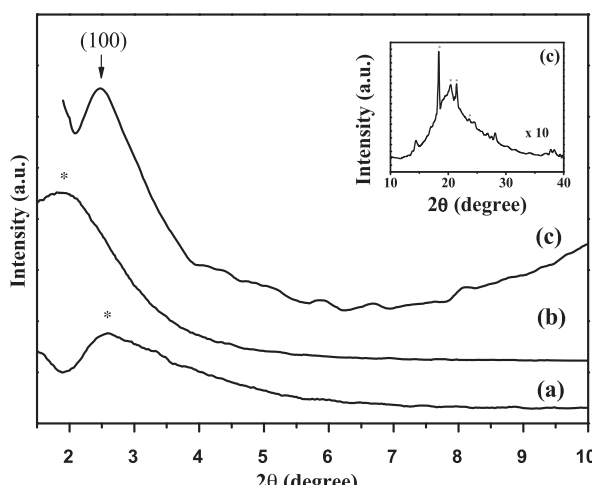


**Fig. 3.** XRD pattern of calcined synthesized (a) MESO-SAPO-34, (b) MESO-SAPO-5, (c) MESO-SAPO-37-0.43S and higher angle XRD pattern of MESO-SAPO-37-0.43S (inset).

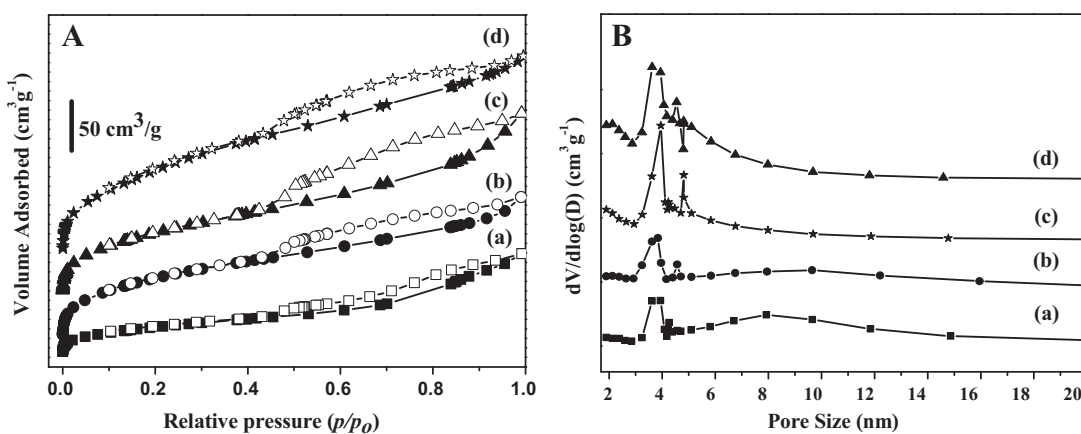


**Fig. 4.** N<sub>2</sub> adsorption/desorption isotherms (A) and pore size distribution (B) for (a) MESO-SAPO-37-0.43S, (b) MESO-SAPO-37-0.50S (c) MESO-SAPO-37-0.60S and (d) MESO-SAPO-37-0.80S.

### 3.2. 1-Octene hydroisomerization

Vapor-phase hydroisomerization of 1-octene was studied in the temperature range 300–450 °C with different WHSV (weight hourly space velocity). The major products obtained for all the catalysts were linear octene (2-octene, 3-octene, and 4-octene), methylheptene, and dimethylhexenes. The reactions proceeded via double-bond shift followed by skeletal rearrangement [34]. Fig. 7 shows the conversion of 1-octene at different temperatures

over the MESO-SAPO-37-0.43S catalyst with a WHSV of 8 h<sup>-1</sup>. The results showed a slight decrease in conversion in the initial hours. The observed deactivation at 300 °C in the initial hours in catalytic activity can be attributed to coke formation at strong acidic sites [47,48,12,49], as clearly shown by the thermo gravimetric analysis (TGA-DTA) of spent catalysts (Fig. 8). The TGA study shows about ~8 wt.% weight loss on the spent catalyst in the temperature range 300–1200 °C (Fig. 8), with corresponding exothermic peak on DTA indicative of soft coke present on the surface of strong acidic sites. The nature of the coke was further analyzed by *diffuse reflectance infrared Fourier transform spectroscopy (DRIFTS)*, which revealed that the observed vibrational bands around 2800–3000 cm<sup>-1</sup> were typical of aliphatic (CH<sub>3</sub>-, CH<sub>2</sub>-type) in nature (Fig. ES1) [50,51]. Fig. 9 clearly shows that the conversion of 1-octene linearly increased with increasing reaction temperature and reached a maximum of 89% yield at 400 °C. Further, an increase in the reaction temperature to 450 °C slightly decreased the conversion of 1-octene owing to the formation of more cracked products at higher temperatures and deactivation of some strong acidic sites. Over the entire temperature range, linear alkenes (2-octene, 3-octene, and 4-octene) were obtained as the major products (~70% yields). The maximum yield of branched isomer products, 33%, was obtained at 400 °C. The maximum 1-octene conversion and selectivity of branched products were obtained at 400 °C; thus, further studies were carried out at this temperature.

The effect of different WHSV at 400 °C was studied over MESO-SAPO-37-0.43S, and the results are shown in Fig. 10. At a WHSV of 12 h<sup>-1</sup>, the conversion of 1-octene was ~83%, which increased to 89% with a decrease in the WHSV to 8 h<sup>-1</sup>. The increase in the conversion was accompanied by a decrease in the WHSV because the reactant molecules had sufficient time to contact active catalytic surfaces and thus afforded high conversion rates. However, a further decrease in the WHSV from 8 to 5 and 2.6 h<sup>-1</sup> decreased the conversion of 1-octene owing to coke formation, blocking the active sites and mesoporous channels. To understand the importance of silica, MESO-SAPO-37 catalysts synthesized with different silica contents were studied for the hydroisomerization of 1-octene at 400 °C and 8 h<sup>-1</sup> WHSV; the results are shown in Fig. 10. When the silica content was varied, the conversion of 1-octene did not vary largely, even though MESO-SAPO-37-0.80S showed relatively less conversion compared to other samples, which might be due to the presence of large silica islands [52]. The selectivity of branched alkenes (Fig. 10b) was comparable for both MESO-SAPO-37 with a low silica and silica-rich MESO-SAPO-37. This is probably because

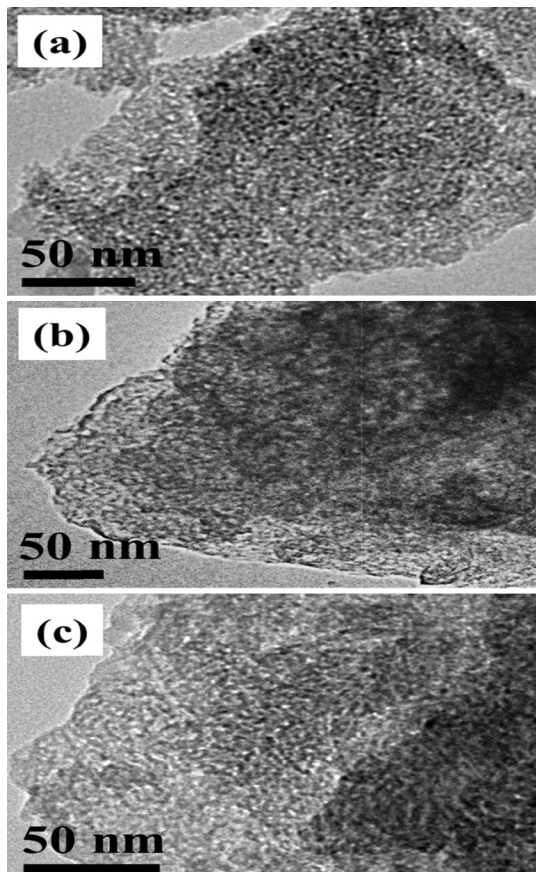


**Fig. 5.** HRTEM images of (a) MESO-SAPO-37-0.43S, (b) MESO-SAPO-5 and (c) MESO-SAPO-34.

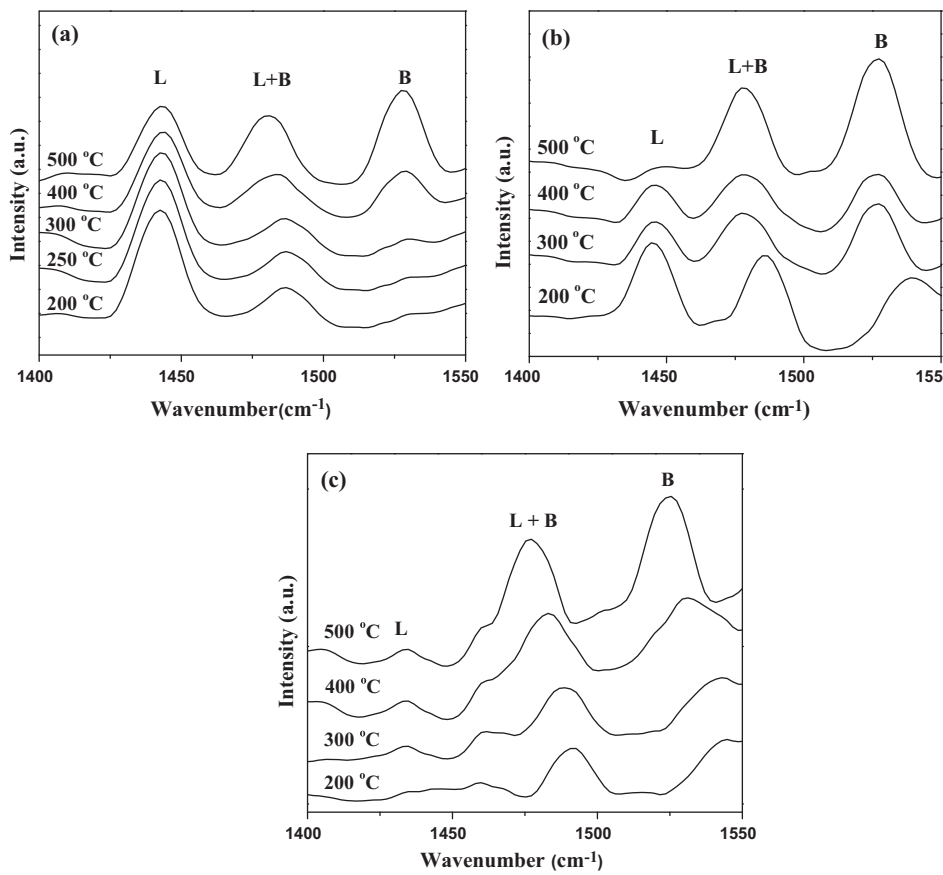


**Fig. 6.** FTIR Pyridine desorption spectra of (a) MESO-SAPO-37, (b) MESO-SAPO-34, and (c) MESO-SAPO-5.

the strong interactions of isolated active silica sites with the reactants leading to skeletal isomerization and formation of similar branched alkenes.

The catalytic activities of other mesoporous analogs were compared by maintaining the temperature (400 °C) and WHSV (8 h<sup>-1</sup>) under identical conditions; the results are shown in Fig. 10. The conversion of 1-octene decreased in the order: MESO-SAPO-37 > MESO-SAPO-5 > MESO-SAPO-34. Furthermore, the selectivity of branched to linear isomerization products (Fig. 10b) decreased in the order: MESO-SAPO-34 ~ MESO-SAPO-37 > MESO-SAPO-5. The branched isomer products were of similar range over MESO-SAPO-37 and MESO-SAPO-34, may be resulted due to presence of strong

Lewis and Brønsted acidic sites together. The catalytic activity was further compared to microporous SAPO analogs, and the results are shown in Table 2. Clearly, both microporous SAPO-34 and SAPO-5 catalysts show relatively less conversion and branched isomer selectivity owing to the small pore opening of SAPO-34 and one-dimensional pore structure of SAPO-5. In contrast, although the faujasite-type SAPO-37 catalyst showed less conversion than the corresponding mesoporous analog, the selectivity of branched isomers is in the similar range due to the three-dimensional large pore opening of the framework. In summary, the presence of strong Lewis and Brønsted sites on MESO-SAPO-37 and mesoporous channel favored the conversion of 1-octene

**Table 2**

Catalytic activity of various silicoaluminophosphate (SAPO) materials on hydro-isomerization of 1-octene<sup>a</sup>.

Catalysts	1-Octene Conversion (%)	Product Selectivity (%)					
		Linear octenes			Branched octenes		
		2-Octene	3-Octene	4-Octene	Methyl-heptenes	Dimethyl-hexenes	
MESO-SAPO-37-0.43 S	88.5	12.3	28.8	24.6	23.5	10.6	
MESO-SAPO-37-0.5 S	82.6	10.6	26.5	29.8	21.3	11.6	
MESO-SAPO-37-0.8 S	84.3	8.9	28.7	26.0	19.1	17.1	
MESO-SAPO-34	79.6	6.9	25.4	26.4	15.8	23.5	
MESO-SAPO-5	87.4	20.3	16.1	40.1	20.9	2.6	
SAPO-37	79.6	8.4	20.2	27.1	16.1	23.3	
SAPO-34	71.7	4.5	25.2	8.5	2.8	28.1	
SAPO-5	64.8	18.4	47.5	29.5	2.1	2.5	

<sup>a</sup> Reaction condition: temperature = 400 °C, WHSV = 8 h<sup>-1</sup> at TOS = 3 h.

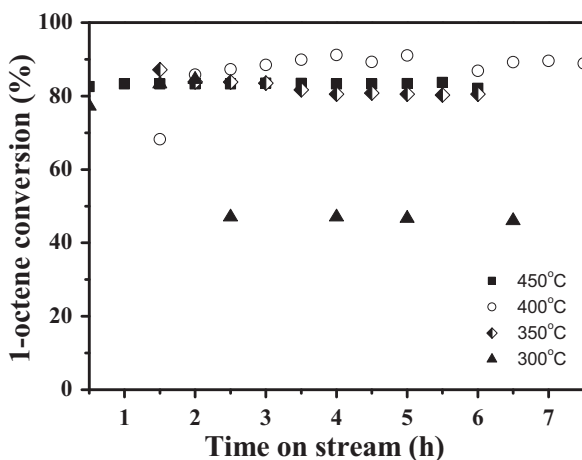


**Fig. 7.** Effect of reaction temperature on 1-octene conversion over MESO-SAPO-37-0.43S at  $\text{WHSV}=8 \text{ h}^{-1}$ .

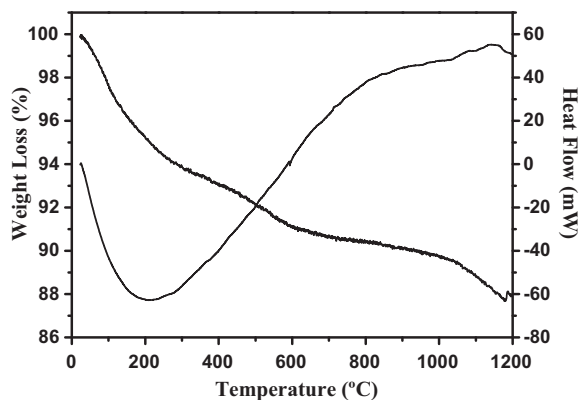


**Fig. 8.** TG/DTA profile of spent catalyst.

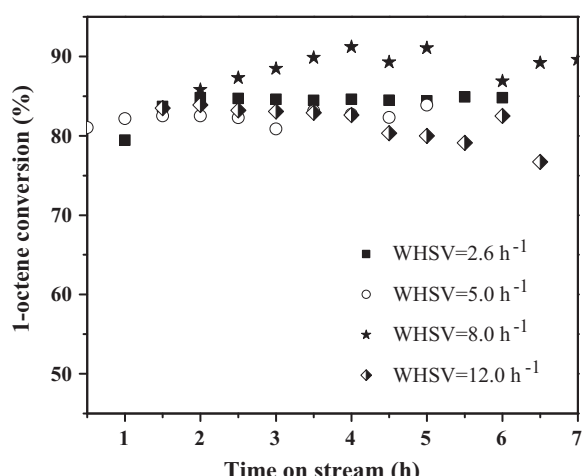


**Fig. 9.** Role of WHSV on 1-octene conversion over MESO-SAPO-37-0.43S at  $400^\circ\text{C}$ .

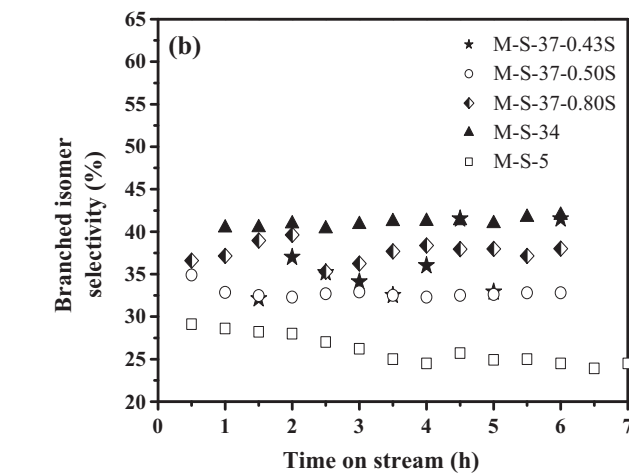
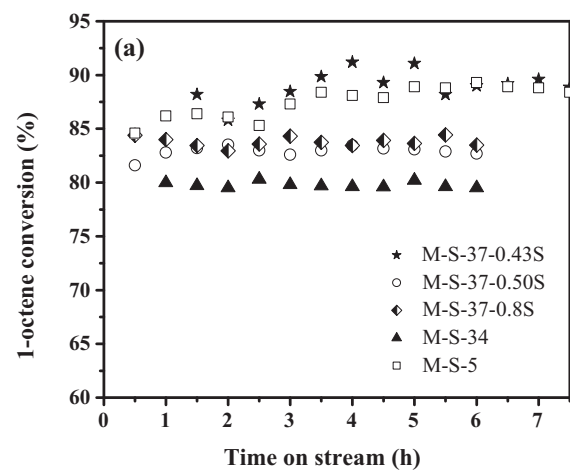


**Fig. 10.** Role of different MESO-SAPO-*n* on hydroisomerization of octene at  $400^\circ\text{C}$  with  $\text{WHSV}=8 \text{ h}^{-1}$ , (a) 1-octene conversion and (b) branched isomer selectivity (where M-S-34=MESO-SAPO-34, M-S-5=MESO-SAPO-5, M-S-37=MESO-SAPO-37).

compared to other systems with comparable branched isomer selectivity.

#### 4. Conclusion

MESO-SAPO-37, MESO-SAPO-34, and MESO-SAPO-5 were synthesized from the corresponding microporous precursors of SAPO-*n*. The mesoporosity of the samples was clearly evident from the powder XRD and  $\text{N}_2$ -sorption studies. The FT-IR analysis supported the presence of microporous structural building unit of the resulting materials. The MESO-SAPO-37-0.43S catalyst showed a better conversion for 1-octene hydroisomerization with the maximum branched products of  $\sim 33\%$ . The presence of strong Brønsted and Lewis acidic sites favored the observed high conversion of 1-octene with good branched isomer selectivity.

#### Acknowledgments

Authors express their sincere thanks to UGC (no. 41-237/2012/(SR)) and DST (SR/S1/PC-11/2011) India for the financial support. Authors are also thankful to USIC, University of Delhi, for the support on instrumentation facility and Dr. R. Nagarajan, University of Delhi for his support on use of powder XRD facility under DST(Nano Mission). RY and AKS are grateful to UGC and CSIR, India for their junior and senior research fellowship respectively.

## Appendix A. Supplementary data

Supplementary data associated with this article can be found, in the online version, at <http://dx.doi.org/10.1016/j.cattod.2014.09.026>.

## References

- [1] B.L. Evering, *Adv. Catal.* 6 (1954) 197–239.
- [2] C. Marcilly, *J. Catal.* 216 (2003) 47.
- [3] Y. Ono, *Catal. Today* 81 (2003) 3.
- [4] J.L. White, M.J. Truitt, *Prog. Nuclear Magn. Reson. Spectrosc.* 51 (2007) 139.
- [5] A.F. Cronstedt, *Kongl Vetenskaps Acad. Handl. Stockholm* 17 (1756) 120.
- [6] S.T. Wilson, B.M. Lok, C.A. Messina, T.R. Cannan, E.M. Flanigen, *J. Am. Chem. Soc.* 104 (1982) 1146.
- [7] J. Yu, R. Xu, *Chem. Soc. Rev.* 35 (2006) 593.
- [8] B.M. Lok, C.A. Messina, R.L. Patton, R.T. Gajek, T.R. Cannan, E.M. Flanigen, *J. Am. Chem. Soc.* 106 (1984) 6092.
- [9] H.O. Pastore, S. Coluccia, L. Marchese, *Annu. Rev. Mater. Res.* 35 (2005) 351.
- [10] J. Sauer, K.-P. Schröder, V. Termath, *Collect. Czech. Chem. Commun.* 63 (1998) 1394.
- [11] R. Yadav, A. Sakthivel, *Appl. Catal. A* 481 (2014) 143.
- [12] C.M. López, L. Ramírez, V. Sazo, V. Escobar, *Appl. Catal. A* 340 (2008) 1.
- [13] I. Fechete, Y. Wang, J.C. Védrine, *Catal. Today* 189 (2012) 2.
- [14] C.-H. Geng, F. Zhang, Z.-X. Gao, L.-F. Zhao, J.-L. Zhou, *Catal. Today* 93–95 (2004) 485.
- [15] W. Liu, T. Shang, Q. Zhou, J. Ren, Y. Sun, *J. Rare Earths* 27 (2009) 937.
- [16] C.T. Kresge, M.E. Leonowicz, W.J. Roth, J.S. Beck, *Nature* 359 (1992) 710.
- [17] D. Zhao, J. Feng, Q. Huo, N. Melosh, G.H. Fredrickson, B.F. Chmelka, G.D. Stucky, *Science* 279 (1998) 548.
- [18] Q. Huo, D.I. Margolese, U. Ciesla, P. Feng, T.E. Gier, P. Sieger, R. Leon, P.M. Petroff, F. Schüth, G.D. Stucky, *Nature* 368 (1994) 317.
- [19] P.T. Tanev, T.J. Pinnavaia, *Science* 267 (1995) 865.
- [20] J.L. Vivero-Escoto, Y.-D. Chiang, K.C.-W. Wu, Y. Yamauchi, *Sci. Technol. Adv. Mater.* 13 (2012) 013003.
- [21] S. Oliver, A. Kuperman, N. Coombs, A. Lough, G.A. Ozin, *Nature* 378 (1995) 47.
- [22] A. Sakthivel, S.K. Badamali, P. Selvam, *Micropor. Mesopor. Mater.* 39 (2000) 457.
- [23] A. Sakthivel, P. Selvam, *J. Catal.* 211 (2002) 134.
- [24] A. Sakthivel, S.E. Dapurkar, N.M. Gupta, S.K. Kulshreshtha, P. Selvam, *Micropor. Mesopor. Mater.* 65 (2003) 177.
- [25] A. Sakthivel, J. Zhao, F.E. Kühn, *Micropor. Mesopor. Mater.* 86 (2005) 341.
- [26] A. Sakthivel, J. Zhao, M. Hanzlik, A.S.T. Chiang, W.A. Herrmann, F.E. Kühn, *Adv. Synth. Catal.* 347 (2005) 473.
- [27] M. Montoya-Urbina, D. Cardoso, J. Pérez-Pariente, E. Sastre, T. Blasco, V. Fornés, *J. Catal.* 173 (1998) 501.
- [28] T. Blasco, A. Chica, A. Corma, W.J. Murphy, J. Agúndez-Rodríguez, J. Pérez-Pariente, *J. Catal.* 242 (2006) 153.
- [29] L. Guo, X. Bao, Y. Fan, G. Shi, H. Liu, D. Bai, *J. Catal.* 294 (2012) 161.
- [30] N. Daniilina, F. Krumeich, J.A.V. Bokhoven, *J. Catal.* 272 (2010) 37.
- [31] P. Mériadeau, V.A. Tuan, F. Lefebvre, V.T. Nghiem, C. Naccache, *Micropor. Mesopor. Mater.* 26 (1998) 161.
- [32] R. Yadav, A.K. Singh, A. Sakthivel, *Chem. Lett.* 42 (2013) 1160.
- [33] A.K. Singh, R. Yadav, A. Sakthivel, *Micropor. Mesopor. Mater.* 181 (2013) 166.
- [34] A.K. Singh, R. Yadav, V. Sudarsan, K. Kishore, S. Upadhyayula, A. Sakthivel, *RSC Adv.* 4 (2014) 8727.
- [35] Y. Fan, X. Bao, D. Lei, G. Shi, W. Wei, J. Xu, *Fuel* 84 (2005) 435.
- [36] L.S. de Saldaña, C. Saldaña, M.E. Davis, *J. Am. Chem. Soc.* 109 (1987) 2686.
- [37] A.F. Ojo, J. Dwyer, J. Dewing, K. Karim, *J. Chem. Soc. Faraday Trans.* 87 (1991) 2679.
- [38] K.-H. Schnabel, G. Finger, J. Kornatowski, E. Löffler, C. Peuker, W. Pilz, *Micropor. Mater.* 11 (1997) 293.
- [39] A.M. Prakash, S. Unnikrishnan, *J. Chem. Soc. Faraday Trans.* 90 (1994) 2291.
- [40] J.L. Falconer, M.A. Carreon, S. Li, R.D. Noble, *U.S. Patent* 2012, US 8,302,782 B2.
- [41] R.D. Shannon, C.T. Prewitt, *Acta Crystallogr. B* 25 (1969) 925.
- [42] D. Zhao, C. Nie, Y. Zhou, S. Xia, L. Huang, Q. Li, *Catal. Today* 68 (2001) 11.
- [43] M. Kruk, M. Jaroniec, *Chem. Mater.* 13 (2001) 3169.
- [44] K.S.W. Sing, D.H. Everett, R.A.W. Haul, L. Moscou, R.A. Pierotti, J. Rouquérol, T. Siemieniewska, *Pure Appl. Chem.* 57 (1985) 603.
- [45] T. Mathew, K. Sivarajanji, E.S. Gnanakumar, Y. Yamada, T. Kobayashi, C.S. Gopinath, *J. Mater. Chem.* 22 (2012) 13484.
- [46] K. Sivarajanji, C.S. Gopinath, *J. Mater. Chem.* 21 (2011) 2639.
- [47] Y. Seo, S. Lee, C. Jo, R. Ryoo, *J. Am. Chem. Soc.* 135 (2013) 8806.
- [48] J.-H. Wang, C.-Y. Mou, *Catal. Today* 131 (2008) 162.
- [49] N. Kumar, J.I. Villegas, T. Salmi, D.Yu. Murzin, T. Heikkilä, *Catal. Today* 100 (2005) 355.
- [50] Y. He, Y. He, *Catal. Today* 74 (2002) 45.
- [51] P.L. Benito, A.G. Gayubo, A.T. Aguayo, M. Olazar, J. Bilbao, *Ind. Eng. Chem. Res.* 35 (1996) 3991.
- [52] L. Guo, Y. Fan, X. Bao, G. Shi, H. Liu, *J. Catal.* 301 (2013) 162.